Tribology International 189 (2023) 108964

Contents lists available at ScienceDirect

Tribology International

journal homepage: www.elsevier.com/locate/triboint

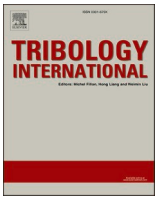

Velocity dependence of barrel friction

P. Sequard-Base [a], A. Koch [b], C. Müller [c], S.J. Eder [d,e,*], J. Sequard-Base [f]

[a] Armaments and Defense Technology Agency (ADTA), Austrian Armed Forces, Roßauer Lände 1, 1090 Vienna, Austria
[b] Federal Office of Armament armasuisse Science and Technology, Feuerwerkerstraße 39, 3602 Thun, Switzerland
[c] WayFound GmbH, Dreistetten 292, 2753 Markt Piesting, Austria
[d] AC2T research GmbH, Viktor Kaplan Straße 2C, 2700 Wr. Neustadt, Austria
[e] Institute of Engineering Design and Product Development, TU Wien, Lehárgasse 6, Objekt 7, 1060 Vienna, Austria
[f] Ballistix Academy e.U., Rittschein 19, 8362 Übersbach, Austria

ARTICLE INFO

Keywords:
Internal ballistics • barrel friction • transversal asperity vibrations • gas pressure curves
5.56 × 45 assault rifle

ABSTRACT

A tribological model is presented that provides a correlation between bullet velocity and friction force in firearms. The model is based on the observation that higher velocities result in lower friction and assumes that the surfaces of the bullet and barrel consist of elastic asperities. The model predicts that as the relative velocity increases, the asperities are less likely to return to their neutral positions. The model was tested using experimental muzzle velocity and gas pressure measurements for caliber 5.56 × 45 bullets and the results were in good agreement with the model predictions. The coefficient of friction obtained with the model is also in line with literature values for very low sliding velocities.

1. Introduction

When it comes to internal ballistics, especially in case of small arms, the frictional forces between the bullet jacket and the inner barrel surface play an essential, but often underestimated role. In the literature, however, only simplified approaches are found [1], or friction is neglected for lack of precise data or knowledge of the underlying phenomena. In the Rheinmetall pocketbook [2], for example, friction is assumed to be constant and independent of the actual bullet velocity (coefficient of sliding friction). This method is also used for the calculation of the leading edge forces on a projectile given in the Oerlikon pocketbook [3].

In connection with questions on the wear of gun barrels, the frictional energy, which is also a major cause of this wear, plays an important role. This becomes especially important in case of lead-free and lead-reduced ammunition, which has become more and more popular over the last two decades in civil, law enforcement, as well as in military use [4–13].

Part of the frictional energy is stored in the form of lattice defects in the surface layer of the barrel material [14–17]. If this successively increasing accumulated energy exceeds a material-dependent limit value, a small particle is detached. More details can be found in [18].

Another important aspect of internal ballistics deals with the energy balance of the gunshot. Here, the frictional energy is also important, as illustrated in Ref. [19]. However, it is often the only parameter that can be determined neither directly in experiments, nor by way of a meaningful theoretical approach.

In the course of the development of special projectiles that have a reduced external ballistic range and thus a reduced hazard area, the need for a deeper theoretical understanding of the phenomenon of velocity-dependent barrel friction also becomes virulent. In these projectiles, part of the frictional energy is deposited in the bullet jacket during the acceleration of the projectile in the barrel, which then partially melts the bullet core during flight. In this way the external ballistic range is shortened by means of a resonance effect.

The development work of such special projectiles impose the need for an in-depth understanding of the frictional processes between bullet and barrel at different velocity regimes.

2. The principle of the model

2.1. The model idea

The surfaces of the bullet jacket and the inner surface of the barrel are modeled with so-called asperities, spatially narrowly defined cylindrically symmetrical bodies with dimensions in the order of a few tenths

* Corresponding author at: AC2T research GmbH, Viktor Kaplan Straße 2C, 2700 Wr. Neustadt, Austria.
E-mail address: stefan.j.eder@tuwien.ac.at (S.J. Eder).

https://doi.org/10.1016/j.triboint.2023.108964
Received 26 January 2023; Received in revised form 24 July 2023; Accepted 16 September 2023
Available online 20 September 2023

of a micrometer. If such an asperity of the moving bullet jacket hits an asperity of the barrel, it is bent until it comes free again ("slips through") and then vibrates at its eigenfrequency. These oscillations are dampened and continue until either the initial resting position is reached or the next barrel asperity is struck. In the latter case, the projectile asperity is bent again. The energy stored in the bent asperity dissipates as heat into the volume of the jacket material during the dampened oscillatory motion. Exactly this energy loss now corresponds to the frictional heat contribution of a projectile asperity on its path in between two barrel asperities assumed in the model. The sum of these losses of vibrational energy of all bullet asperities after the passage of the entire barrel thus corresponds to the frictional energy absorbed by the projectile. The behavior of a single barrel asperity in the face of the bullet asperities passing it is analogous. Thus, the sum of the vibrational energy losses of all barrel asperities constitutes the frictional energy in the barrel. These two energies therefore add up to the total internal ballistic frictional energy during the shot.

2.2. Basic assumptions

In order to keep the modelling analytically clear, the following simplifying assumptions are made:

- The asperities of the bullet jacket and the inner surface of the barrel are geometrically represented by a cylindrically symmetric combination of a longer truncated cone as the main body and a substantially shorter cone placed on top of it. The wide base of such a cone is firmly connected to the respective base material and thus also determines an upper limit for the areal density of the asperities. The lengths of the cones and their bottom diameters can be different, related to each of the two tribosurfaces, but they are kept constant for each tribopartner. The top diameter of the truncated cones and the heights of the attached cones are, however, the same for both tribopartners. This chosen geometric representation of the asperities is done for ease of calculating their vibrations, and because it allows them to have a smaller height in relation to the bottom diameters of the attached cones. In accordance with Greenwood and Williamson [20], these geometric relations of the attached cones represent the real asperity better. The longer truncated cone is thought to be inside the substrate, and its consideration is necessary to obtain suitable frequencies for the vibrations. The form of an elastic cone is necessary for calculations concerning small displacements when two surfaces are interacting under pressure.

- A uniform hypothetical radius of curvature (radius of the spherical cap) R_k is assumed for all asperities. This is done to simplify the description of the pressure interaction between the two tribosurfaces. The spherical cap is represented, in a further simplified form in the model, as that cone which is placed on the truncated cone body. Therefore, the top diameters of the cones of the projectile and barrel must also be the same. Fig. 1 sketches the geometrical conditions.

Since the curvature radius R_k and the radius of the top surface r is the same for all involved cones, also the cone height h is the same for all cones of the model asperities.

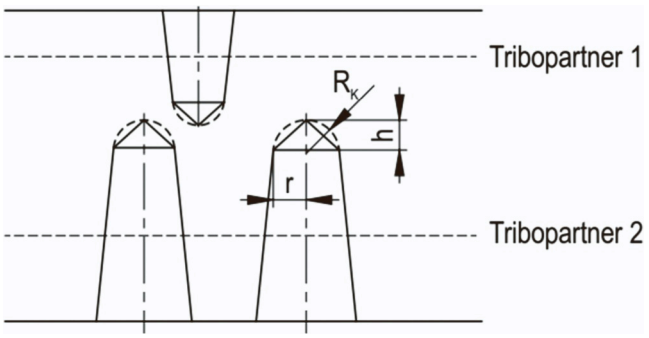

Fig. 1. Sketch of the basic geometry of the cones used in the model for the outer surface of the bullet and the inner surface of the barrel, referred to here as tribopartners 1 and 2, respectively.

$$h = R_K \left(1 - \sqrt{1 - \left(\frac{r}{R_K} \right)^2} \right) \tag{1}$$

- The dynamic modeling of an asperity is carried out according to the physical-mechanical laws of a unilaterally clamped conical rod by means of numerical methods. The required spring and damping constants are thus defined, taking into account the respective material properties. It is always assumed that the elastic range is not exceeded for any bends occurring in the asperities. Only under these boundary conditions, the approach of a harmonic oscillator for the modelling of the bending vibrations is permissible. From the literature, an approach is known in which the behavior of a tribosurface is described via the oscillation of springs [21].

- The geometrical arrangement of the asperities on a tribopartner is always assumed to be homogeneous (here as a chessboard-like regular arrangement of the asperities). The alignment of the chessboard-like grids of the two asperity fields is always thought to be parallel to each other and also parallel to the direction of movement of the projectile in the barrel. With this simplification, on the one hand, a constant distance between the asperities is defined and, on the other hand, a strictly periodic mechanical sequence of the bending, e.g., of a projectile asperity, is defined. This asperity then interacts strictly periodically with the barrel asperities equivalent to teeth in a rack.

- The chessboard arrangement of the asperities does not correspond to their actual physical arrangement, but rather represents an averaged arrangement of the asperities.

- The surface densities of the asperities are constant for each tribopartner. However, they can be set differently in relation to each other (bullet-to-barrel).

- From the above simplifications it also follows that the (average) maximum bending amplitudes A_0 of the asperities at the moment of "release" after the contact phase of an asperity with an opposing asperity are also constant for each material.

Remark:

In the strict rack-like case, the A_0-amplitudes necessarily correspond to the geometrically possible maximum values. However, since in reality the asperities are not arranged along straight lines, it follows that the interacting asperities do not only strike "centrally" but also "laterally" and can therefore "come free" at even smaller amplitudes than the absolute maximum amplitudes just mentioned. Thus, A_0 is the average maximum amplitude when "coming free".

- In the model, the force of a barrel asperity on a passing projectile asperity corresponds to a force F acting perpendicular to the longitudinal axis of the asperity, which can be represented as:

$$F = k\,x \tag{2}$$

with k the spring constant and x the current deflection of the asperity tip.

- The oscillation that starts after bending is described by Eq. 3:

$$x = A_0\, e^{-\frac{t}{\tau}} \cos \omega\, t \tag{3}$$

with τ the time constant of the damping and ω the angular frequency of the asperity oscillation.

2.3. Calculation of the friction energy

The geometrical relations of a projectile asperity moving at velocity v during the encounter with two barrel asperities is shown in Fig. 2, and the corresponding oscillation of the asperity in Fig. 3.

The oscillation period Δt between two asperity contacts, which are generally spatially separated by the distance d (no index is used here, since it is independent whether barrel or bullet), thus results in

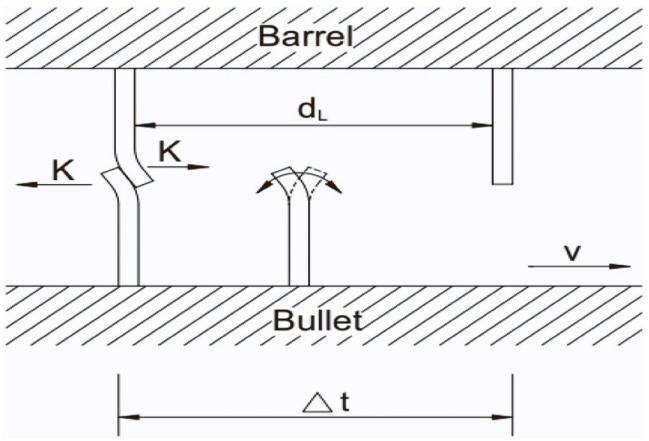

Fig. 2. A projectile asperity moves with velocity v past a barrel asperity (left part of the figure), or between two barrel asperities (middle part of the figure). The asperities are represented here symbolically as simple rods, despite the fact that they are considered as truncated cones with cones on top. Let the distance between two barrel asperities be d_L. The time between two asperity contacts Δt can be calculated based on this distance and the velocity.

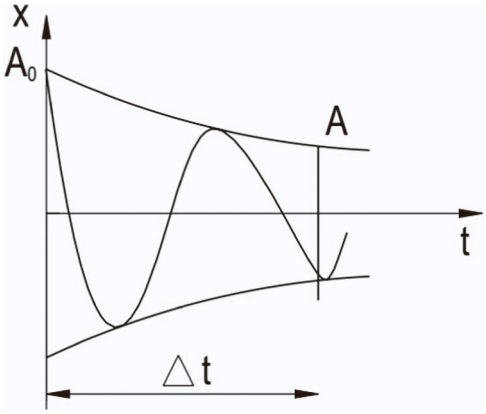

Fig. 3. The damped vibration of a bullet asperity between contacts with two barrel asperities.

$$\Delta t = \frac{d}{v} \tag{4}$$

The mean deflection of the asperity at the time of "release" after contact with an asperity of the other tribopartner is A_0. At the time of the contact with the next asperity, let the mean amplitude now be A. As can be seen from Fig. 3, A is therefore the value of the enveloping curve at time Δt, and not the amplitude value corresponding to the formal oscillation according to Eq. 3. This approach is chosen because A_0 is a mean maximum value and therefore a mean maximum value must be used for A as well.

The mean energy ΔE_1 emitted by a single asperity during the oscillation time Δt results from the decrease of its mean bending, as Fig. 4 shows (index 1 due to reference to a single asperity).

The following applies:

$$d\Delta E_1 = F\,dx \tag{5}$$

With Eq. 2 one obtains after integration

$$\Delta E_1 = \frac{k}{2}\left(A_0^2 - A^2\right) \tag{6}$$

Since A is the value of the enveloping function it follows with

$$x = A_0\, e^{-\frac{t}{\tau}}$$

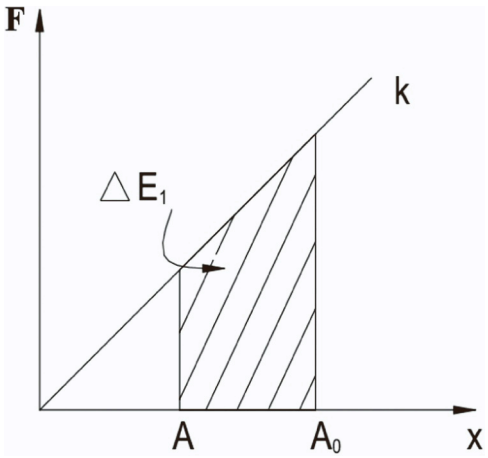

Fig. 4. The mean dissipated energy of a single asperity in the force-displacement diagram.

and considering Eq. 4.

$$A = A_0\, e^{-\frac{\Delta t}{\tau}} \tag{7}$$

ultimately:

$$\Delta E_1 = \frac{k}{2} A_0^2 \left(1 - e^{-\frac{2}{\tau}\frac{d}{v}}\right) \tag{8}$$

Eq. 8 provides the average energy dissipated by an asperity between two contacts with asperities of the respective opposite tribopartner.

In order to obtain the total frictional energy absorbed by the barrel and the bullet, estimates must be made of the numbers of involved asperities on the two tribosurfaces. For this purpose, both the inner surface of the barrel and the contact surface of the bullet jacket are cut open lengthwise and considered as two flat rectangles. In the following considerations, a smooth bore is assumed for simplification. Section 2.6 gives the equations for the conditions in a rifled barrel with a land and groove profile.

In the following, the indices L for barrel and G for bullet and the following denominations apply:

ρ_{AL} Asperity density of the barrel,
ρ_{AG} Asperity density of the bullet,
N Number of asperities of the unfolded inner surface of the barrel,
M Number of asperities of the opened contacting surface of the bullet jacket,
n Number of asperities of the barrel in axial direction,
m Number of asperities of the bullet contacting surface in the axial direction,
i Number of asperities of the barrel perpendicular to the axial direction,
j Number of asperities of the bullet contacting surface perpendicular to the axial direction,
D Caliber,
L Tribologically relevant barrel length,
l Length of the projectile contacting the surface.

According to Fig. 5, the following applies.

$N = \rho_{AL}\, L\, D\, \pi$ and $N = n\, i$ as well as $\frac{i}{n} = \frac{D\,\pi}{L}$.

from which

$$n = L\sqrt{\rho_{AL}} \tag{9}$$

follows, and analogously (according to Fig. 6) one obtains

$$m = l\sqrt{\rho_{AG}} \tag{10}$$

Thus, the distance d between two barrel asperities can also be written in the form

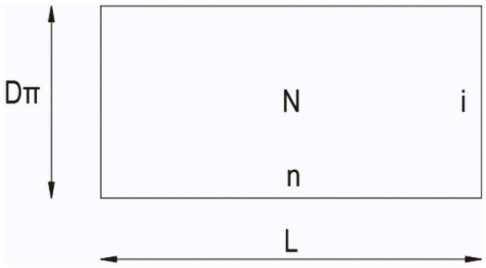

Fig. 5. Unfolded inner barrel surface.

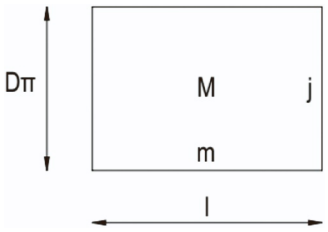

Fig. 6. Unfolded projectile contacting surface.

$$d = \frac{L}{n} = \frac{1}{\sqrt{\rho_{AL}}} \tag{11}$$

Again, in the idealized way of the chessboard arrangement of the asperities along a single rack, each one of the m projectile asperities interacts with all n barrel asperities, so the dissipated energy ΔE_Z can be given as

$$\Delta E_Z = m\, n\, \Delta E_1$$

The number r of the azimuthal racks (and thus of mutually parallel racks) of the projectile and the barrel that effectively interact with each other are taken as the minimum of the values i and j,

$$r = Min(i,j)$$

From

$$i = \frac{N}{n} = \sqrt{\rho_{AL}}\, D\, \pi \tag{12}$$

and analogously

$$j = \frac{M}{m} = \sqrt{\rho_{AG}}\, D\, \pi \tag{13}$$

the total frictional energy absorbed by the projectile is E_{RG}:

$$E_{RG} = r\, m\, n\, \Delta E_1 \tag{14}$$

and therefore

$$E_{RG} = \sqrt{Min(\rho_{AL},\rho_{AG})}\, \frac{\pi}{2}\, D\, L\, l\, k_G\, A_{0G}^2\, \sqrt{\rho_{AL}\cdot\rho_{AG}}\left(1 - e^{-\frac{2}{\sqrt{\rho_{AL}}\,\tau_G\,v}}\right) \tag{15}$$

Similarly, the total frictional energy absorbed by the barrel is given by E_{RL} to:

$$E_{RL} = \sqrt{Min(\rho_{AL},\rho_{AG})}\, \frac{\pi}{2}\, D\, L\, l\, k_L\, A_{0L}^2\, \sqrt{\rho_{AL}\cdot\rho_{AG}}\left(1 - e^{-\frac{2}{\sqrt{\rho_{AG}}\,\tau_L\,v}}\right) \tag{16}$$

Thus, according to this model, the total interior ballistic relevant frictional energy E_R is equal to:

$$E_R = E_{RG} + E_{RL} \tag{17}$$

The division of frictional energy between barrel and bullet is done using the specific asperity data and not, as sometimes found in literature by using the ratio of thermal conductivities of barrel and bullet materials. The thermal conductivities are only responsible for the further dissipation of the thermal energy, i.e., the frictional energy, away from the friction interface.

In a first rough approximation of the total frictional energy, the energy contributions of the barrel and the projectile can be assumed to be equal, i.e. $E_{RG} \sim E_{RL}$. However, this also means that:

$$P_A = P_{AG} = P_{AL}$$

$$k = k_G = k_L$$

$$\tau = \tau_G = \tau_L$$

$$A_0 = A_{0G} = A_{0L}$$

Accordingly, from Eqs. 15, 16, and 17, we obtain the total friction energy to be:

$$E_R = \sqrt{\rho_A}\, \rho_A\, \pi\, D\, L\, l\, k\, A_0^2 \left(1 - e^{-\frac{2}{\sqrt{\rho_A}\,\tau\,v}}\right) \tag{18}$$

The corresponding frictional force F_R follows as

$$F_R = \frac{\partial E_R}{\partial L} = \sqrt{\rho_A}\, \rho_A\, \pi\, D\, l\, k\, A_0^2 \left(1 - e^{-\frac{2}{\sqrt{\rho_A}\,\tau\,v}}\right) \tag{19}$$

In its simplest form, Eq. 19 describes the dependence of the total frictional force on the current projectile velocity inside the barrel.

2.4. Modelling the pressure conditions between the bullet and the inner surface of the barrel

Before the projectile is forced into the barrel by the action of the hot powder gases, its outer diameter (measured in the region of the guiding surface) is slightly larger than the inner barrel diameter (here again assumed to be a smooth bore). After the bullet leaves the cartridge, the bullet is pressed to the nominal inside barrel diameter along a section of the barrel called forcing cone. During this process, the bullet is deformed both plastically and elastically both in the jacket and in the core. The elastic deformation is associated with a contact pressure of the bullet against the barrel. This is absolutely critical for obtaining sufficient gas sealing so that the hot powder gases behind the projectile can accelerate the bullet through the barrel as efficiently as possible. The barrel, made of steel, is assumed to be rigid in these considerations. For each approved caliber, there are standardized values in the European area listed in the CIP (Commission Internationale Permanente Pour L'Eupreves des Arms a Feu portatives) and in the American area given in the SAAMI (Sporting Arms and Ammunition Manufacturers' Institute) for the maximum cartridge and bullet outer diameter before firing and the minimum chamber and barrel inner geometry, as well as for maximum chamber pressures [22,23]. From these data, an approximation of the contact pressure p can be made. This raises the question of where this pressure p is represented in the equations of the presented model (e.g., Eq. 19 for the frictional force).

To answer this question, at first the parallel motion of the projectile inside the barrel is left aside and only a movement of two tribosurfaces perpendicular to each other is considered. This approach has to be done for calculation of the overlap s. Therefore, it is possible to get the mean maximum bending amplitude A_0, which will represent the pressure p in the model. It is additionally assumed that the two asperities moving toward each other initially engage in contact "point to point". As they approach each other, the tips then slide on the respective opposite lateral surfaces, thus pushing the cones together and, at the same time, somewhat to the side. A certain force or energy is required for this transverse bending of the two asperities under consideration. The higher the contact pressure, the more the asperities bend until an energy equilibrium is reached. An additional simplification within the model is that the cone surfaces have no friction. The product of the macroscopic contact pressure p with the macroscopic surface S (this is the surface of

the bullet along the contacting length) results in the normal force F_N. The movement of the two tribosurfaces in relation to each other, beginning with the first contact of the cones involved, finally ends, precisely in the state of equilibrium, after a vertical distance s has been covered. Via the product of F_N times s, one finally obtains the energy which, on the one hand, is macroscopically introduced into this compression and, on the other hand, as seen in the model, is now stored in the transverse bending of the asperities. At the same time, this distance s corresponds to the "overlap" between the cones of the asperities, as can be seen in Fig. 7 on the left side.

Remark. : If the two tribosurfaces then slide in parallel (as is the case during the shot), the asperities then have to bend further than in the case of a purely perpendicular motion until they "release" each other (slip) in order to subsequently oscillate with their damped eigenfrequency. Thus, the (average) maximum amplitude A_0 is determined for a first qualitative approximation.

For a quantitative consideration, the first step is to think of the bullet jacket (guiding surface) and the inner surface of the barrel again "cut open" and "unrolled" lengthwise, i.e., as two flat surfaces. Furthermore, it is again assumed that these two surfaces, as discussed above, move perpendicularly towards each other so that they are pressed more and more against each other. The effective tribosurface of an asperity in the model as a conical tip placed on a rotationally symmetrical cone. Fig. 7 shows this simplified geometry at the end of the vertical approach by highlighting the distance s. The tribosurfaces of an asperity pair (here now generalized with indices 1 and 2) as well as the acting forces can be seen.

F_0 corresponds to the normal force acting on the macroscopic bodies, and F_{0i} is its share of the i-th asperity pair. Based on the right part of Fig. 7, the normal force F_N (relative to the lateral surfaces of the cone) and the horizontal forces F_{H1} and F_{H2} are obtained within the framework of a force analysis:

$$|F_N| = |F_{0i}|\sin\alpha \quad F_{H1} + F_{H2} = 0 \quad |F_{H1}| = |F_{H2}| = |F_N|\cos\alpha$$

and thus:

$$|F_{H1}| = |F_{H2}| = |F_{0i}|\sin\alpha\cos\alpha \tag{20}$$

The two bodies press on each other with p over the surface S, i.e.,

$$p = \frac{F_0}{S} \tag{21}$$

where the surface S, due to the asperity surface density ρ_A [$\rho_A = \mathrm{Min}(\rho_{AL}, \rho_{AG})$] contains exactly N_0 asperities. However, the force F_o is not distributed over all N_0 asperities, but only over a part of them. This fraction of contributing asperities is determined by the factor f (which will be explained in more detail later). For the actually interacting asperities N, one therefore obtains:

$$N = \rho_A S f$$

With respect to a pair of asperities, Eq. 21 applies to the force F_{0i}

$$F_{0i} = \frac{F_0}{N} = \frac{F_0}{\rho_A S f} = \frac{p}{\rho_A f} \tag{22}$$

The amplitudes A_1 and A_2 of the transverse deflection of the asperities follow via the horizontal forces as

$$|F_{H1}| = |F_{H2}| \quad \Rightarrow \quad k_1 A_1 = k_2 A_2 \tag{23}$$

and under the effect of the contact pressure p, using Eqs. 20, 22 and 23 as:

$$A_1 = \frac{p \sin\alpha\cos\alpha}{\rho_A f k_1} \quad A_2 = \frac{p \sin\alpha\cos\alpha}{\rho_A f k_2} \tag{24}$$

The energy E_i stored by the contact pressure p per pair of asperities is obtained from the force displacement diagram of a mechanical harmonic oscillator with

$$E_i = \frac{k_1 A_1^2}{2} + \frac{k_2 A_2^2}{2} \tag{25}$$

This is also connected with the "convergence", i.e., the overlap s of the two opposite asperities (see also Fig. 7 left) for which applies in the same way:

$$E_i = F_{0i}\, s \tag{26}$$

Eqs. 20, 23, 25 and 26 then yield s for the overlap

$$s = \frac{A_1 + A_2}{2} \sin\alpha\cos\alpha \tag{27}$$

With the expressions for the amplitudes according to Eq. 24, it follows for s that

$$s = \frac{p\,(\sin\alpha\cos\alpha)^2}{2\,\rho_A f}\left(\frac{1}{k_1} + \frac{1}{k_2}\right) \tag{28}$$

As mentioned earlier, when the two tribosurfaces move vertically with respect to each other, not all asperities of both surfaces will interact with each other. To take this into account, the factor f was introduced. A simple estimation of this factor will be discussed in the following. It is assumed from the probability that two asperities located on opposite tribosurfaces can touch each other due to geometrical conditions. The theoretically "possible" area corresponds to the area S_i assigned to each individual asperity on average due to the given area density of the asperities. It results from the reciprocal value of the area density of the asperities ρ_A. If the number of asperities is set equal to 1, it follows

$$S_i = \frac{1}{\rho_A} \tag{29}$$

So the tip of one asperity has to be within a specific area so it can contact an opposing asperity. This area is a circle with the radius r_S, corresponding to an area A_i. The size of this area is now related to the overlap s calculated in the model. Fig. 7, left part, shows the geometry of two asperities at the end of the vertical movement towards each other, i.e., when the overlap s is reached.

Note that in the presented calculation model.

- a constant height of the asperities (cone height) is assumed and.
- the determination of the overlap distance s assumes the "first contact" in the geometric constellation "point to point".

This implies that all involved asperity pairs are always "bent" equally. The extent of the real bending, however, depends on where on the jacket surface the two opposite asperity cones actually make geometric contact for the first time. The amount of bending is then proportional to the distance along the vertical line that starts from the point of this first contact on the jacket surface and ends at the point of intersection of this

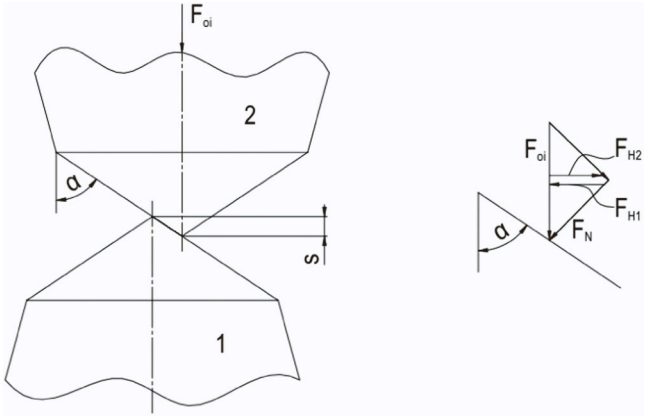

Fig. 7. The end of the "vertical encounter" of an asperity pair (i-th pair) after reaching the distance s (left) and the simplified split of forces (right).

line on the bottom surface of the cone. This distance thus corresponds to a weighting of the bending at this (random) horizontal displacement of the first contact of the two asperity tips. The total volume of the upper part of the cone (see also Fig. 8 the highlighted cone part) thus corresponds to the sum of all weights for the different bendings based on the actual geometrical encounter of two cones. Since the overlap s should be the same for all points of contact, the actual geometric cone is formally replaced by a volume-equal cylinder with the height s. Due to the volume equality, the sum of the weights is preserved. Fig. 8 shows this situation schematically.

For sake of clarity: First the calculation for s according to Eq. 28 as well as the angle α and the radius of the cone deck r is performed. This defines the (model) cone. Now, on the basis of the volume equality between the actual geometrically overlapping upper cone part (cone apex with height h_s) and the computationally relevant cylinder, the value for this radius of the cylinder r_s is determined. According to Fig. 8 the similarity is valid:

$$\frac{h_s}{r_s} = \frac{h}{r} \tag{30}$$

From this and the volume equality (V_K denoting the volume of the cone and V_z denoting the volume of the cylinder)

$$V_K = \frac{r_s^2\,\pi\,h_s}{3} = r_s^2\,\pi\,s = V_z \tag{31}$$

Follow

$$h_s = 3\,s \tag{32a}$$

$$r_s = \frac{3\,s\,r}{h} \tag{32b}$$

According to Eq. 32a, the actual "geometric" overlap h_s is now larger than the overlap s calculated in the model, but the two overlaps are physically equivalent.

For the horizontal area A_i within which the two vertically engaging asperity peaks must be located, Fig. 9 delivers the following:

$$A_i = r_s^2\,\pi = \frac{9\,r^2\,s^2\,\pi}{h^2} \tag{32}$$

Only if the two asperity peaks are at a horizontal distance smaller than or equal to r_S, a contact at a given vertical approach of the – calculated – length s is possible at all. Now it is assumed for the case of this vertical approach that if the tip of, e.g., the lower cone is spatially

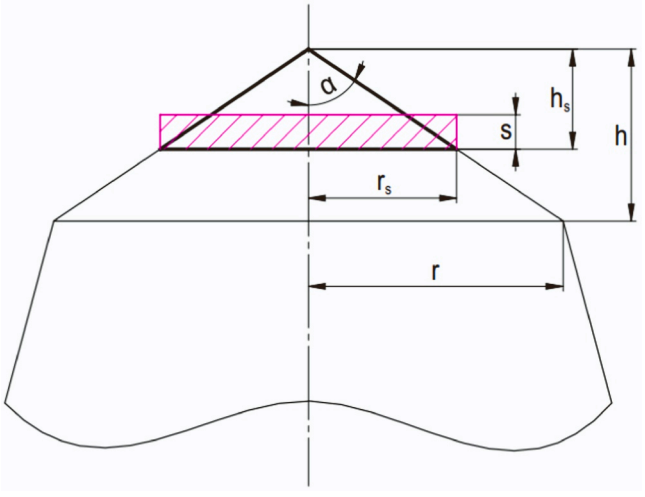

Fig. 8. On the actual geometry of the asperity cone involved in the contact (bold line) and its associated volume-equivalent cylinder (colored pink) from the point of view of equality of statistical weights for the bends in an effectively random asperity–asperity encounter constellation.

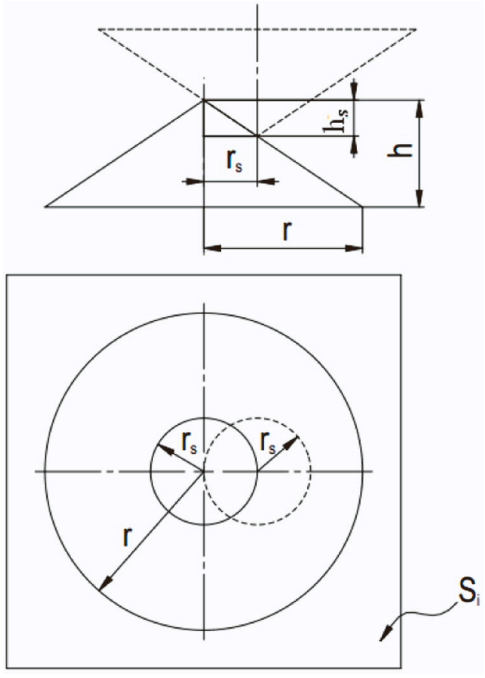

Fig. 9. The "physical-geometric" conditions for the contact of the two asperity peaks. Shown here is the geometric position for the largest possible horizontal distance r_s of the two asperity tips for a given geometric overlap h_s.

fixed in the plane, the tip of the upper cone takes a random position within the horizontal plane of the lower tribopartner. The probability of contact therefore corresponds to the areal ratio f between the area A_i and the possible area S_i.

$$f = \frac{A_i}{S_i} = \frac{9r^2\pi s^2\rho_A}{h^2} \tag{33}$$

Therefore,

$$N = f\,N_0 \tag{34}$$

asperities are affected, which either bend maximally when the tips meet each other head-on, or where there is only glancing contact when the horizontal distance between the tips is just r_S. This would account for the physical reality within the model discussed here.

For the trigonometric term in Eq. 28, the following is also valid:

$$(\sin\alpha\,\cos\alpha)^2 = \frac{r^2\,h^2}{\left(r^2 + h^2\right)^2} \tag{35}$$

Thus, the overlap s in the state of energy equilibrium is obtained when the pressure p acts and the materials are the same, i.e., $k = k_1 = k_2$ via Eqs. 28, 33, 35 and considering that $h << r$, to:

$$s = \sqrt[3]{\frac{p\,h^4}{9\,\pi\,\rho_A^2\,r^4\,k}} \tag{36}$$

Remark:

The question arises whether this effort for obtaining the factor f is really necessary, since in the course of the simplifications inherent in every model the approach to the asperity contact "point-to-point" could simply be fixed and all asperities of the two tribopartners encounter each other in this way. However, this is not the case. It turns out that the overlap s obtained in this way is too low and therefore unrealistic mean bending amplitudes A_0 are obtained when the projectile moves through the barrel (see later).

The chessboard-like arrangement of the asperities in simplified form and the parallel alignment of these "chessboards" between the

tribopartners projectile and barrel prove their worth in the modeling of the translatory projectile motion in the barrel. However, for the consideration of the contact pressure, i.e., the vertical movement of the tribosurfaces towards each other, the neglect of the random horizontal displacement of the two surfaces with respect to each other would not be permissible.

In summary, the following applies: Based on the contact (interaction) of two surfaces with similar, transversely moving asperities, separately from each other.

- on one hand the corresponding behavior of the contact pressure (movement of the two surfaces towards each other with factor *f*) is modeled and
- on the other hand, the behavior of friction is calculated when the two surfaces move parallel to each other.

2.5. The evaluation of A_0

The normal pressure p between the bullet jacket and the inner surface of the barrel causes the asperities to "interlock" with the overlap s. The mean maximum vibration amplitude of the asperities A_0 at the time of "release/slip" during the sliding motion of the two tribosurfaces has to be evaluated. The determination of these vibration amplitudes, in general for two different cones on the two tribosurfaces, is carried out on the basis of the geometric relationships shown in Fig. 10. The two cones differ, according to the conditions of this modeling, in their length and with their spring constant (as well as the vibration damping duration). The overlap s is calculated according to the explanations in Section 2.4, again with the initial condition of "point-to-point" first contact of opposing asperities (effect of the contact pressure p).

Here, the asperities differ in their lengths L_1 and L_2 as well as in their spring constants k_1 and k_2, which thus lead to a different distribution of the overlap s with the parts x_1 and x_2 (see Fig. 10). This is also associated with different maximum amplitudes A_{01} and A_{02}. The following equations apply

$$(L_1 - x_1)^2 + A_{01}^2 \cong L_1^2 \text{ geometric position according to Fig.10} \tag{37}$$

$$(L_2 - x_2)^2 + A_{02}^2 \cong L_2^2 \text{ geometric position according to Fig.10} \tag{38}$$

$$x_1 + x_2 = s \text{ overlap due to contact pressure } p \tag{39}$$

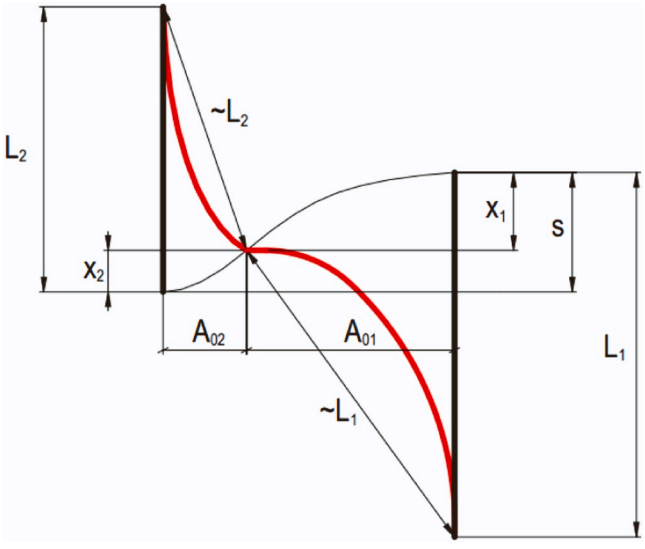

Fig. 10. Two geometrically and materially different asperities sliding against each other shortly before "release" with given overlap s (red denotes the bending situation; the red straight lines indicate the neutral positions).

$$k_1 A_{01} = k_2 A_{02} \text{ equilibrium of forces.} \tag{40}$$

For physical-geometric reasons, x_1, x_2, s, $<< L_1$, L_2. Neglecting all terms of order greater than or equal to 2, Eqs. 37–40 give for the maximum amplitudes:

$$A_{01} = \sqrt{\frac{2\,L_1\,L_2\,s}{L_2 + L_1\left(\frac{k_1}{k_2}\right)^2}} \tag{41}$$

$$A_{02} = \sqrt{\frac{2\,L_1\,L_2\,s}{L_2\left(\frac{k_2}{k_1}\right)^2 + L_1}} \tag{42}$$

For the case of equal asperities on both sides of the tribosurface, it follows because of:

$L_1 = L_2 = L$ and $k_1 = k_2 = k$ that

$$A_{01} = A_{02} = \sqrt{L\,s} \tag{43}$$

2.6. Consideration of the land-groove profile in the barrel

Eqs. 15 and 16 for the friction energies apply, as already indicated, to a smooth bore barrel. However, in the small caliber segment, rifled barrels are usually used. Different pressures prevail between the bullet and the barrel, depending on whether a contact occurs on the land or in the groove of the barrel. The rifled barrel according to CIP is defined by the groove width b_Z and the number of grooves N_Z. D now corresponds to the land diameter, and the different pressures are accounted for by the different mean amplitudes A_0. In the present model, no twist angle is considered. Furthermore, the indices F for land and Z for groove are used. Based on the equations for the smooth bore (see Section 2.3), Eqs. 15 and 16 are modified for the frictional energies in the projectile and in the barrel as follows.

$$E_{RG} = \sqrt{Min(\rho_{AL},\rho_{AG})}\,\sqrt{\rho_{AL}\cdot\rho_{AG}}\,\frac{L\,l}{2}\,k_G\left[D\,\pi\,A_{0G,F}^2 - N_Z\,b_Z\left(A_{0G,F}^2 - A_{0G,Z}^2\right)\right]\left(1 - e^{-\frac{2}{\sqrt{\rho_{AL}}\,\tau_G\,v}}\right) \tag{44}$$

$$E_{RL} = \sqrt{Min(\rho_{AL},\rho_{AG})}\,\sqrt{\rho_{AL}\cdot\rho_{AG}}\,\frac{L\,l}{2}\,k_L\left[D\,\pi\,A_{0L,F}^2 - N_Z\,b_Z\left(A_{0L,F}^2 - A_{0L,Z}^2\right)\right]\left(1 - e^{-\frac{2}{\sqrt{\rho_{AG}}\,\tau_L\,v}}\right) \tag{45}$$

3. The model in context with experimental data from firing tests

3.1. General overview

It is known in expert circles that the absolute value of the total friction energy generated by a bullet during its motion inside the barrel, under otherwise identical conditions such as barrel geometry and bullet design, becomes higher the lower the muzzle velocity v_0 is [24]. A variation of the muzzle velocity is realized via different charges, i.e., practically by varied quantities of powder. For the experimental verification of the model just presented, the 5.56 × 45 caliber with the Swiss GP90 cartridge was selected. The caliber 5.56 × 45 is currently the most common caliber for assault rifles worldwide.

In a first step, measurements of the gas pressure curves as well as of v_0 were carried out at armasuisse on a test barrel system in caliber 5.6 mm using a GP90 bullet with different charges [24]. Based on these curves, the motion of the bullet until it leaves the barrel was now determined by calculation. With the aid of a simple first approach of a friction force that shall be assumed independent of the current velocity of the projectile, i.e., constant throughout the barrel, it is then shown that such a force must tend to be higher the lower v_0 is. The frictional forces must be taken into account to obtain the respective v_0 values.

Without the introduction of friction, the muzzle velocity calculated from the gas pressure curve would otherwise exceed the measured muzzle velocity, sometimes significantly. The experimental muzzle velocities in this test series is in the interval from approx. 450–900 m/s.

In addition to these tests, so-called quasi-static push-through tests at the ADTA of the Austrian Armed Forces were performed [25]. Here, projectiles were slowly (i.e., quasi-statically) pressed through a barrel with the aid of a universal testing machine, and thus the frictional force is determined at a very low sliding velocity (approx. 1 mm/s) via a force-displacement measurement.

In the next step, again based on the measured gas pressure curves, the above-mentioned approach for calculating the bullet motion in the barrel is supplemented with the algorithm of the velocity-dependent friction model presented here. For simplicity and clarity, geometrically and materially identical asperities are assumed for the barrel and for the bullet. The material parameters are taken as the arithmetic averages of steel (for the barrel) and copper (for the bullet jacket). Thus, the four parameters ρ_A (asperity surface density), k (spring constant), τ (damping constant), and A_0 (mean maximum asperity deflection at the time of release of a "bent" asperity) describe what happens in the velocity-dependent friction model. These four parameters are now varied over a wide range with the aid of a simulation program, and the respective muzzle velocities are calculated with all 20 experimentally obtained gas pressure curves. For each parameter set, a root mean square (RMS) deviation value can now be determined jointly over all 20 gas pressure curves between the v_0 values obtained with the model, relative to the experimentally recorded v_0 values. This is how one obtains the most suitable parameter set.

Finally, based on this best-fit parameter set, an approximation of the asperity geometry is determined. This gives a clearer idea of the morphology of the tribosurfaces in connection with the friction between the projectile and the barrel. For simplicity, an asperity firmly attached to the substrate is assumed. The deviation value (RMS) from the experimental v_0 values is also calculated for this theoretical approximation, based on the 20 test shots (gas pressure curves) mentioned above.

3.2. The experimental tests and their results

The data of the measurement system at armasuisse are summarized in Table 1.

The gas pressure is measured using a piezo pressure sensor, which measures the chamber pressure inside a drilled cartridge case. The determination of the muzzle velocities takes place via two light barriers (more precisely the velocity at a distance of 5 m from the muzzle). In order to realize different muzzle velocities, four different powder charges were used, with powder masses of 0.85 g, 1.0 g, 1.2 g, and 1.6 g. Five shots were then measured for each powder mass.

Fig. 11 shows the 20 measured gas pressure curves and the v_0 obtained for each gas pressure curve. Note the different scales.

Fig. 12 shows the test setup for the quasi-static push-through tests together with the results (force-displacement diagrams) in Fig. 13.

Averaging the force–displacement profiles given in Fig. 13, for a barrel length of 46 cm, gives the mean frictional force $\langle F_R \rangle$ and therefore, the mean energy $\langle E_R \rangle$ of:

$$\langle F_R \rangle = 2093 \pm 198\ \text{N} \quad \langle E_R \rangle = 963 \pm 91\ \text{J}$$

Table 1
General data on the measuring system.

Barrel length (mm)	464
Bullet travel in the barrel (mm)	428.6
Land diameter (mm)	5.55
Groove diameter (mm)	5.69
Twist length (mm)	177.8
Initial bullet motion without rotation (mm)	max. 1.5
Bullet weight*) (g)	4.082
Bullet diameter (mm)	5.7

*) The bullet is taken from a Swiss GP90 cartridge.

Remark:

In the push tests, M193 type bullets were used instead of the GP90 projectiles. It should also be noted that the projectile is pushed through the barrel by the universal testing machine via a slightly under-caliber push rod. This is intended to avoid extensive friction of the push rod against the inner wall of the barrel. In practice, however, it is inevitable that the push rod will bend somewhat as a result of the applied pressure and thus contribute to the friction, albeit only over a small area. However, the fact that the push rod bends somewhat also means that part of the compressive force is contained in this bending and not exclusively in the friction. An exact and reliable quantitative estimate of all these superimposed effects is not possible.

3.3. Bullet kinematics in the barrel

Starting from the measured gas pressure curves $p(t)$, the expressions

$$(m_G + \varepsilon\, m_P)\, \frac{d}{dt} v(t) = S\, p(t) - F_R \tag{46a}$$

$$\frac{d}{dt} x(t) = v(t) \tag{46b}$$

With:
m_G bullet mass,
m_P powder mass,
ε Sebert factor,
S bullet cross-section (= barrel inner cross-section), and
F_R frictional force.

The velocity $v(t)$ and the respective location of the projectile $x(t)$ are calculated numerically. The distance the projectile has to travel until it reaches the muzzle is 428.6 mm.

In the first approach, the frictional force F_R is assumed to be a constant, i.e., independent of the current velocity. This shows that for each of the four used powder masses m_P, a different average value must be used for the frictional force F_R, so that the projectile leaves the muzzle mathematically with the experimentally measured v_0. These results are listed in Table 2.

According to Table 2, it is evident that there can be no friction force independent of the actual bullet velocity. The higher the measured v_0, the smaller the (constant) friction force for calculating this v_0 from the gas pressure curves has to be.

Thus, as a second approach, instead of a constant frictional force, the velocity-dependent frictional force according to Eq. 19 is now used in the expression 46a for the numerical determination of v_0. Eq. 19 is a simplification of the presented model, in the sense that tribologically identical conditions are assumed for both the inner surface of the barrel and the bullet jacket.

The first task is now to find the parameter set with which, for all four used powder masses and thus for all measured gas pressure curves, the calculated v_0 values determined according to Eq. 46a and b best agree with the actually measured v_0 values. This is done numerically within the ranges of values and increments given in Table 3. A root mean square (RMS) value, with respect to the deviation, is defined as a measure of agreement between the respective measured v_0 data and the calculated v_0 data. Furthermore, with reference to the results of the quasi-static push-through tests, a minimum value for the frictional force of not less than 1600 N is required under these velocity conditions (v ~ 1 mm/s). The purely mathematically determined best fit is also shown in Table 3 (right).

Using the best-fit parameter set, Table 4 compares the v_0 values calculated with it to the actual experimental v_0 values, and also reports the mean frictional force $\langle F_R \rangle$ and the total aggregated frictional energy E_R. The reported mean frictional force $\langle F_R \rangle$ is the mean value of the

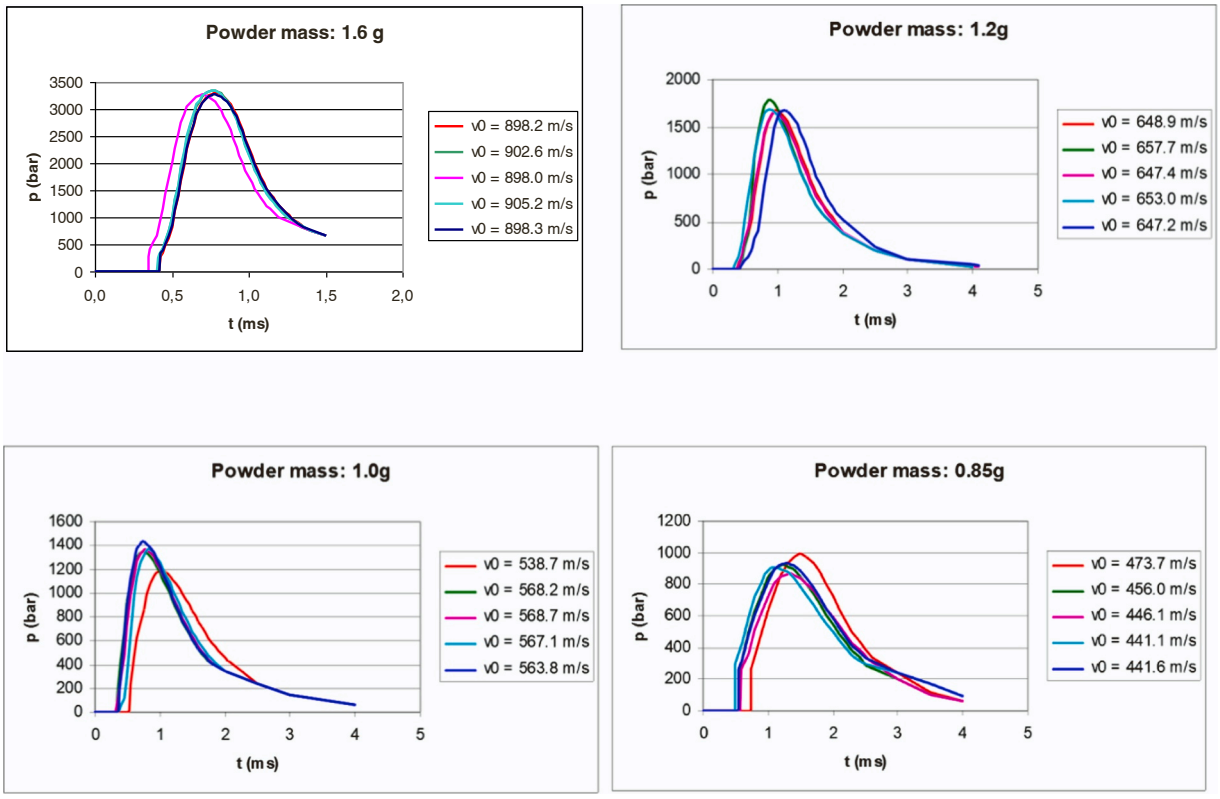

Fig. 11. The measured gas pressure curves and the muzzle velocity v_0 associated with each curve.

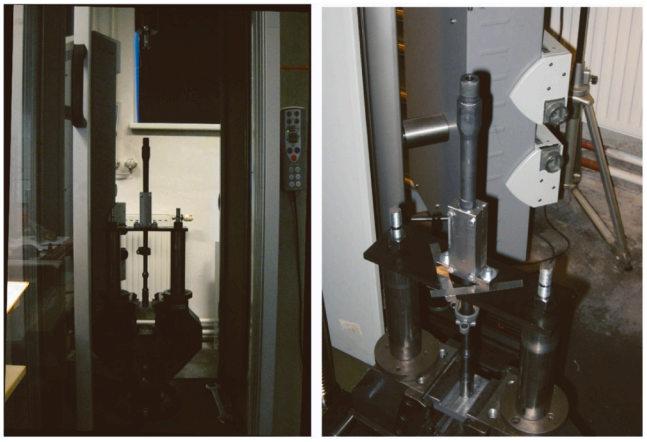

Fig. 12. The universal testing machine with the clamped barrel of a SIG550.

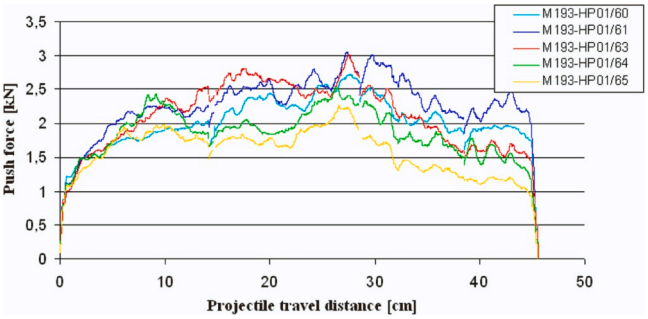

Fig. 13. The push-through force along the barrel of an assault rifle SIG550.

frictional force for each individual shot (the frictional force in the presented model depends on the current velocity of the bullet) and is then averaged over the five shots per powder mass. The other data are always to be understood as averaged only over the five test shots per powder mass.

The relative error f_r of the calculated with respect to the measured v_0 values has to be emphasized in Table 4. It shows the good reproduction of the measured values by the velocity-dependent friction model. However, this best-fit parameter set consists of numerical values found purely by varying the four parameters, without considering any physical-morphological background.

The model however, assumes that the roughness of the tribosurfaces is governed by asperities, which are excited to transverse oscillations by the projectile motion. Therefore, an attempt is made to calculate the transverse vibration behavior of conically shaped asperities in order to find an asperity geometry whose vibration parameters are as close as possible to the best-fit parameter set. The calculations for k and τ are carried out for different dimensions of conically shaped, rotationally symmetric, and unilaterally fixed bodies according to [26] and [27].

Table 2
The average values determined by calculation with a constant frictional force F_R, i.e., independent of the current bullet velocity in the barrel, per powder mass used, always as an average value over five shots, as well as the corresponding experimentally measured muzzle velocities v_0.

m_P (g)	0.85	1.0	1.2	1.6
v_0 exp. (m/s)	451.8 ± 13.75	561.4 ± 12.66	650.8 ± 4.71	900.4 ± 3.36
F_R (N)	558 ± 42.8	384 ± 43.5	407 ± 31.3	126 ± 18.5

$$E\,I\,\frac{\partial^4 y}{\partial x^4} + C\,I\,\frac{\partial^5 y}{\partial x^4\,\partial t} + \rho\,S\,\frac{\partial^2 y}{\partial t^2} = F(x,t) \tag{47}$$

With:
E Young's modulus (Pa),

Table 3
Variation ranges and increments for the purely mathematical test of the four model parameters. The best fit obtained in this way yields an $RMS = 17.08$ m/s, and the friction force in the quasi-static case is $F_{R0} = 1602$ N.

Parameter	minimum	maximum	increment	best fit
Asperity density ρ_A (Asp. /μm^2)	0.6	1.1	0.05	0.65
Spring constant k (N/m)	5000	18000	200	14000
Damping time constant τ (ns)	20	80	5	45
Average max. Amplitude A_0 (nm)	30	80	5	50

Table 4
Results with the best-fit parameter set. f_r is the relative error between the calculated and measured v_0 values.

m_P (g)	0.85	1.0	1.2	1.6
v_0 exp. (m/s)	451.8 ± 13.75	561.4 ± 12.66	650.8 ± 4.71	900.4 ± 3.36
v_0 best fit (m/s)	453.6 ± 34.54	569.4 ± 15.57	655.2 ± 7.46	884.0 ± 2.55
f_r (%)	**+ 0.40**	**+ 1.43**	**+ 0.68**	**-1.82**
$\langle F_R \rangle$ (N)	303.0 ± 16.09	234.4 ± 8.82	213.2 ± 4.97	153.8 ± 0.84
E_R (J)	129.9 ± 6.90	100.5 ± 3.78	91.4 ± 2.13	65.9 ± 0.36

I Surface moment of inertia (m^4),
C internal damping (Pa s),
ρ mass density of the cone (kg/m^3),
S cross-section (m^2) of the cone at location x (m), and
$F(x,t)$ shear force per length (N/m).

The arithmetic mean values between steel (barrel) and copper (bullet jacket) are used for the Young's modulus and for the material density. For the internal damping, $C = 1$ Pa s is used. The latter is an assumed approximation, due to the fact that the cone is fixed on one side.

According to Ref. [28], the asperities of a tribosurface interact with each other in a way that they can be assumed as solid particles within an elastic substrate. This is also depicted in the colored shaded parts of Fig. 14. As a result, the mechanical loading of a single asperity via this elastic substrate also affects its neighbors. However, since the elastic substrate is not taken into account here, the additional spring forces and damping associated with these interactions are not represented mathematically. The approximation consists in the exclusive consideration of asperities not interacting with each other in this way within the same tribosurface. This justifies the approach of asperities firmly clamped on one side.

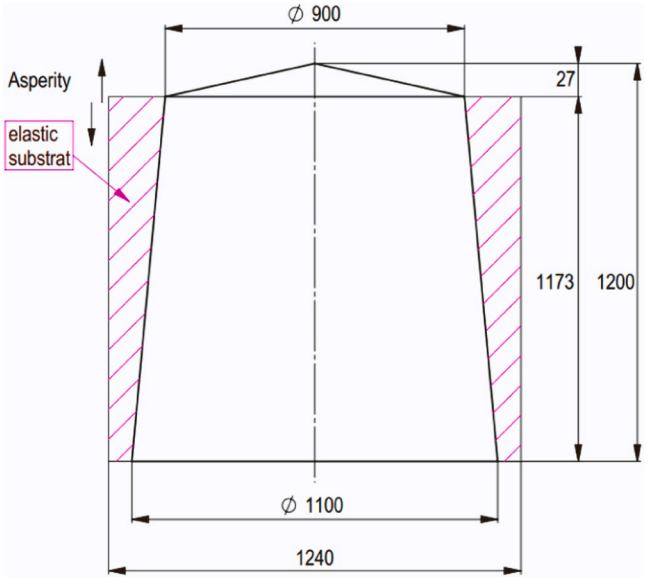

Fig. 14. Illustration of a possible asperity for the calculation of the friction force with the velocity-dependent model. In pink, a possible elastic substrate is indicated, which is not considered here. This may also extend further into the volume of the body below the cone bottom surface. The tribosurface itself would then be a two-dimensional periodic array of such asperity constructions as shown in the figure. The drawing is not to scale, all dimensions given are in nm.

Analogously, the damping C is set to the value of 1 Pa s. In addition, under the given extremely short time scale combined with very high mechanical and thermal loads during the internal ballistic processes of a shot, the actual values of the material parameters are uncertain. The use of material parameters, such as the Young's modulus, with the numerical values as they apply in conventional mechanics (for quantities that change moderately in time) must therefore also be regarded as an approximation here.

The solution of Eq. 47 is performed numerically (for example, the cross-section S of the cone also depends on x and is therefore not a real constant of the equation). Therefore, an analytical solution for the geometry of an asperity that exactly corresponds to the best-fit parameter set is not possible. Only by smart "trial and error", a suitable asperity shape can be found. The transverse force F is applied permanently for determining, e.g., k or only briefly for determining τ.

As such a solution for a simple asperity geometry one obtains, e.g., a cone with an attached cone as sketched in Fig. 14.

The assumed radius of curvature R_K of an asperity is responsible for the ratio of cone height to diameter of the cone bottom. Here, according to [28], an average radius of curvature of $R_K = 3730$ nm was used.

The side length a of the surface part (square) assigned to the cone is given with 1240 nm in Fig. 14 and results from the asperity surface density with

$$a = \sqrt{\frac{1}{\rho_A}} \tag{48}$$

From the calculation with Eq. 47, k and τ are obtained. The asperity surface density is taken from the best-fit parameter set. With an estimated normal pressure of $p \sim 127$ MPa, Eqs. 36 and 43 are used to obtain the value for A_0. Thus, the parameter set for the cone is:

$k = 10907$ N/m
$\tau = 46.5$ ns
$\rho_A = 0.65$ Asperities/μm^2
$A_0 = 53.18$ nm

With these parameters, the v_0 values as well as the average friction forces and friction energies are calculated for all twenty measured gas pressure curves, analogous to the best-fit parameter set. The averaged results for the selected cones are summarized in Table 5, analogous to the best fit results.

If the elastic substrate discussed earlier would be considered, an asperity in this model can also be seen as a flat, but wide elevation. This would then correspond to the top cone alone. In the present case with a height of 27 nm and a diameter of 900 nm. It should be remembered that the actual geometry of such an asperity would be a spherical calotte

Table5
Results with the cone–cone parameter set. Again, f_r is the relative error between the calculated and measured v_0 values.

m_P (g)	0.85	1.0	1.2	1.6
v_0 exp. (m/s)	451.8 ± 13.75	561.4 ± 12.66	650.8 ± 4.71	900.4 ± 3.36
v_0 cone (m/s)	494.6 ± 22.11	581.8 ± 14.13	667.8 ± 5.26	888.8 ± 2.38
f_r (%)	**+ 9.47**	**+ 3.63**	**+ 2.61**	**-1.29**
$\langle F_R \rangle$ (N)	244.8 ± 8.79	196.8 ± 7.36	180.0 ± 4.30	131.0 ± 0.71
E_R (J)	104.9 ± 3.77	84.3 ± 3.15	77.1 ± 1.84	56.1 ± 0.30

with a radius of about 3730 nm. Indeed, the cone represents only the approximation for this spherical calotte.

According to Tables 4 and 5, the relative errors are all less than 2% for the best fit and less than 10% for the cone. Fig. 15 shows the comparison between the experimentally measured v_0 values and the v_0 values calculated with the best fit and the cone on the basis of the velocity-dependent friction model.

In general, the lower the used powder mass, the more irregular the powder combustion will be during the shot. This is reflected in the gas pressure curves. However, the gas pressure curves are the starting point for calculating the bullet kinematics in the barrel. As a result, the respective standard deviation increases with decreasing powder mass, as can also be seen in Fig. 15.

In accordance with the velocity-dependent friction model presented here, Fig. 16 shows the friction force as a function of the current bullet velocity in the barrel.

As Fig. 16 shows, the main differences between the best-fit and the cone–cone design are visible for the lower velocities. This can be explained by the fact that for the cone–cone design, the effects of the elastic substrate are not considered here. In case of the low velocities there are the longest oscillation durations between the contacts of opposing asperities. Therefore the damping influence of the substrate, which is missing in the cone–cone model and would increase the friction losses, has the strongest effect under these conditions.

Finally, a connection is to be made with Amonton's law, which is widely used for the description of friction phenomena between solids. It is valid for the friction force F_R, the normal force F_N and the coefficient of friction μ:

$$F_R = \mu F_N \tag{49}$$

Based on the data valid for the present tests regarding normal pressure p, barrel inside diameter D, and bullet contacting length l with:

$p \sim 127$ MPa

$D = 5.6$ mm

$l = 5$ mm ,

the normal force results in

$F_N = 11.172$ kN.

Since the normal force can be assumed to be constant during the bullet motion, a velocity-dependent coefficient of friction is obtained as shown in Fig. 17. The friction force curve for the best fit (see Fig. 16) is assumed and the coefficient of friction μ is calculated according to Eq. 49.

At (very) low velocities, the coefficient of friction corresponds to the usual coefficients of sliding friction between steel and copper found in literature. For example, Refs. [29,30] give a CoF range of $\mu = 0.10 - 0.17$ for the metal pairing steel - CuSn (dry). According to Ref. [31], the CoF

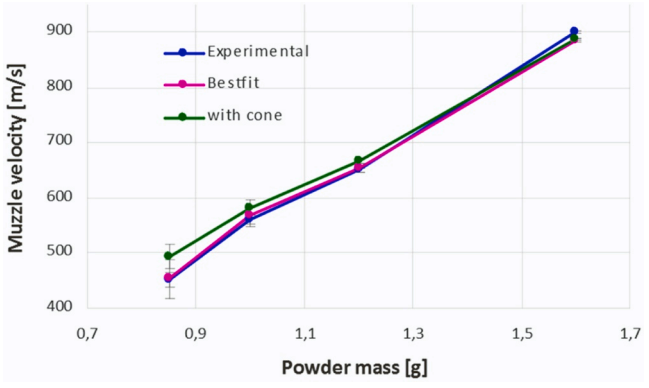

Fig. 15. The experimentally measured v_0 values compared to the calculated v_0 values with the discussed velocity-dependent friction model as a function of the four investigated powder masses. The error bars correspond to the standard deviations of the muzzle velocities.

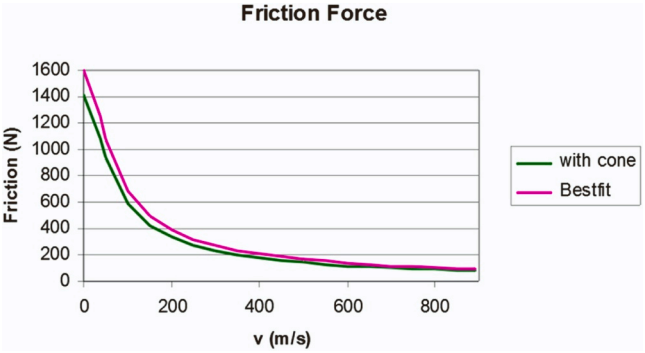

Fig. 16. The decelerating force acting on the bullet moving inside the barrel, depending on the current velocity.

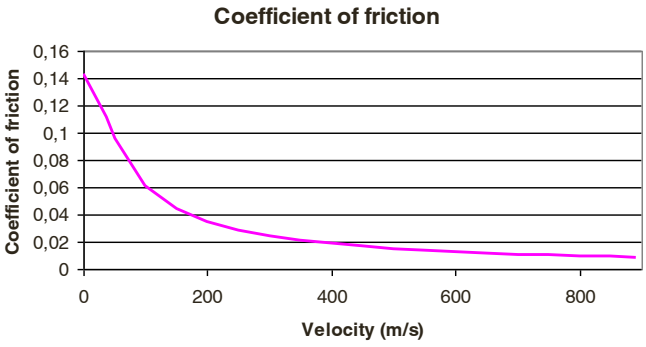

Fig. 17. The coefficient of sliding friction as a function of the current velocity of the bullet in the barrel.

for the material combination steel–Cu, $\mu = 0.15 - 0.68$. This applies at a contact pressure of $p = 10$ MPa and a velocity of $v = 0.1$ mm/s. However, especially at this interval, the specified measuring velocity is not nearly comparable with the velocities that a projectile can reach in the barrel.

The good agreement of

- the sliding coefficients of friction found in the literature with the results of the friction model presented here on the basis of transversely oscillating asperities in the low-speed range (the literature values are only valid there) as well as
- the relatively small error between the measured v_0 values and the v_0 values determined with the friction model on the basis of the experimental gas pressure curves

suggest that the simplified choice of the material parameters (mean values between steel and copper) for the asperity modeling is justifiable. A refinement of the results is conceivable if the corresponding specific material parameters are used for the asperities of the barrel and the projectile jacket, and Eqs. 15 and 16 are used for the modeling.

The next step would be to transfer the presented method to other calibers in order to gain an even deeper insight into high velocity tribology as it exists in the context of internal ballistics of firearms from the comparison of the results there with the results presented here.

An alternative path would be to investigate the phenomenon of friction decrease with increasing velocity using molecular dynamics (MD) simulation. This could involve analyzing possible short-lived and spatially confined melting processes at the nanoscale, as an explanation of a reduction in friction [32]. A consideration of thermal effects, as they are also treated with MD, could refine the presented friction model. In the cone-cone variant, for example, the elastic substrate would change to some degree and thus influence the spring and damping constants of the asperities.

4. Conclusion

As illustrated in the paper, the velocity-dependent friction force model discussed here, based on transverse asperity oscillations, is very well able to describe the experimentally observable friction of the projectiles as they move through the barrel. At low velocities, the coefficients of friction of the velocity-dependent friction force model gives values in the interval of those literature values that were determined elsewhere by measurement on the basis of the well-known Amontons' friction law. From the comparison of the push-through tests with the shooting tests, it can also be deduced that the coefficient of friction must be significantly reduced at high speeds.

Declaration of Competing Interest

The authors declare that they have no known competing financial interests or personal relationships that could have appeared to influence the work reported in this paper.

Data Availability

Data will be made available on request.

Acknowledgements

Special thanks are due to armasuisse of the SWISS ARMY for the experimental support of this work with respect to the firing tests as well as for valuable theoretical suggestions. Special thanks are also due to the Armaments and Defense Technology Agency of the Austrian Armed Forces for the experimental execution of the push-through tests and for making possible the theoretical elaboration of the model. Part of this work was funded by the Austrian COMET-Program (Project K2 InTribology1, no. 872176) and carried out at the "Excellence Centre of Tribology". Open access funding was provided by TU Wien (TUW).

Statement of originality

I declare on behalf of my co-authors that this work is original, and that the submitted manuscript has not been published elsewhere and is not under consideration at any other journal.

References

[1] Boyle, P., Humphrey, A., Proctor, S., Courtney, M. (2012). Measuring Barrel Friction in the 5.56 mm NATO. Air Force Academy Colorado Springs Co.
[2] RHEINMETALL Waffentechnisches Taschenbuch, 8th edition, Düsseldorf, 1989.
[3] OERLIKON Pocketbook, 2nd edition, Zurich, 1981.
[4] Summer P., Courtney M. Friction effects of lead-based and lead-free primers in 5.56 mm NATO" US Air Force Academy Report ADA594429, 2014.
[5] Fox News: Army testing new 'green' bullets. https://www.foxnews.com/tech/army-testing-new-green-bullets [accessed 11th January 2023].
[6] Fox News: End of the line for the lead bullet? Regulations, bans force switch to 'green' ammo. https://www.foxnews.com/us/end-of-the-line-for-the-lead-bullet-regulations-bans-force-switch-to-green-ammo [accessed 11th January 2023].
[7] Kurier: Mannstoppende Polizeimunition gegen Kollateralschäden. https://kurier.at/chronik/oesterreich/mannstoppende-polizeimunition-gegen-kollateralschaeden/401427762 [accessed 11th January 2023].
[8] Avery D, Watson RT. Regulation of lead-based ammunition around the world. Ingestions Lead spent Ammunit: Implic Wildl Hum 2009:161–8.
[9] European chemical agency (2021). Towards sustainable outdoor shooting and fishing – ECHA proposes restrictions on lead use, https://echa.europa.eu/de/-/towards-sustainable-outdoor-shooting-and-fishing-echa-proposes-restrictions-on-lead-use [accessed 11th January 2023].
[10] Green RE, Pain DJ. Risks to human health from ammunition-derived lead in Europe. Ambio 2019;48(9):954–68.
[11] Pain DJ, Dickie I, Green RE, Kanstrup N, Cromie R. Wildlife, human and environmental costs of using lead ammunition: an economic review and analysis. Ambio 2019;48(9):969–88.
[12] Pain DJ, Mateo R, Green RE. Effects of lead from ammunition on birds and other wildlife: a review and update. Ambio 2019;48(9):935–53.
[13] Arnemo JM, Cromie R, Fox AD, Kanstrup N, Mateo R, Pain DJ, et al. Transition to lead-free ammunition benefits all. Ambio 2019;48(9):1097–8.
[14] Mishra A, Hameed A, Lawton B. A novel scheme for computing gun barrel temperature history and its experimental validation. J Press Vessel Technol 2010;132(6).
[15] Ward, J.R., Brosseau, T.L., Grollman, B.B. (1981). Heat Transfer in Guns-Determination of Friction Factor from Heat Input Measurements. Army Ballistic Research Lab Aberdeen Proving Ground MD.
[16] Sorokatyi RV, Dykha AV. Analysis of processes of tribodamages under the conditions of high-speed friction. J Frict Wear 2015;36(5):422–8.
[17] Wang L, Li S, Xu F, Yang G. United computational model for predicting thermochemical-mechanical erosion in artillery barrel considering friction behavior. Case Stud Therm Eng 2022;29:101726.
[18] Sequard-Base J, Lenauer C, Lazarev V, Gavrilov K, Doikin A, Vorlaufer G. A modified energy-based model for describing wear processes applied to an internal combustion engine. Int J Comput Methods Exp Meas 2015;3(2):150–64.
[19] Sequard-Base J, Haas R, Tomastik C, Vernes A, Franek F. Barrel friction in sport rifles. Tribol Lett 2018;66(1):1–10.
[20] Greenwood JA, Williamson JP. Contact of nominally flat surfaces. Proceedings of the royal society of London. Series A. Math Phys Sci 1966;295(1442):300–19.
[21] Popov M, Popov VL, Pohrt R. Relaxation damping in oscillating contacts. Sci Rep 2015;5(1):1–9.
[22] https://www.cip-bobp.org/de/tdcc [accessed 11th January 2023].
[23] https://saami.org/technical-information/ansi-saami-standards/ [Accessed 11th January 2023].
[24] Koch A., Ubertini F., Krebs B. Friction in the barrel, 5.6mm Gw Pat 90. Interim report, armasuisse Science and Technology. Internal report, 2018.
[25] Sequard-Base J., Sequard-Base P. Tribological investigations on internal ballistics for the StG77 as well as StG90, internal report, 2017.
[26] Schwinkendorf KN, Roblyer SP. Simulation of the vibrational response of a rifle barrel during firing. SCS society for computer simulation. Simul Ser 1998;30:66–74.
[27] Harris CM, Piersol AG. Fifth edition. Shock and Vibration Handbook. McGraw-Hill Handbooks; 2002.
[28] Yeo CD, Katta RR, Lee J, Polycarpou AA. Effect of asperity interactions on rough surface elastic contact behavior: hard film on soft substrate. Tribology Int 2010;43(8):1438–48.
[29] Gomeringer, R. , Heinzler, M. , Kilgus, R. , Menges, V. , Näher, F. , Oesterle, S. & et al. (2014). Tabellenbuch Metall. Verlag Europa-Lehrmittel Nourney, Vollmer.
[30] Wittel, H., Muhs, D., Jannasch, D., Voßiek, J. (2017). Roloff/Matek Maschinenelemente. Vieweg+ Teubner Verlag.
[31] Maissen VA. Festkörperreibung-Reibungszahlen verschiedener Werkstoffe. Schweiz Ing und Archit 1993;111(3):25–9.
[32] Eder SJ, Grützmacher PG, Rodríguez Ripoll M, Gachot C, Dini D. Does speed kill or make friction better?—designing materials for high velocity sliding. Appl Mater Today 2022;29:101588.